Journal of Colloid and Interface Science 683 (2025) 722–730

Contents lists available at ScienceDirect

Journal of Colloid And Interface Science

journal homepage: www.elsevier.com/locate/jcis

Regular Article

Tuning the nanostructure and tribological properties of a non-ionic deep eutectic solvent with water addition

Joshua J. Buzolic [a], Matteo Tiecco [b], Rob Atkin [a], Hua Li [a,c,*]

[a] School of Molecular Sciences, The University of Western Australia, Perth, WA 6009, Australia
[b] School of Pharmacy, ChIP Research Center, University of Camerino, Camerino, MC 62032, Italy
[c] Centre for Microscopy, Characterisation and Analysis, The University of Western Australia, Perth, WA 6009, Australia

GRAPHICAL ABSTRACT

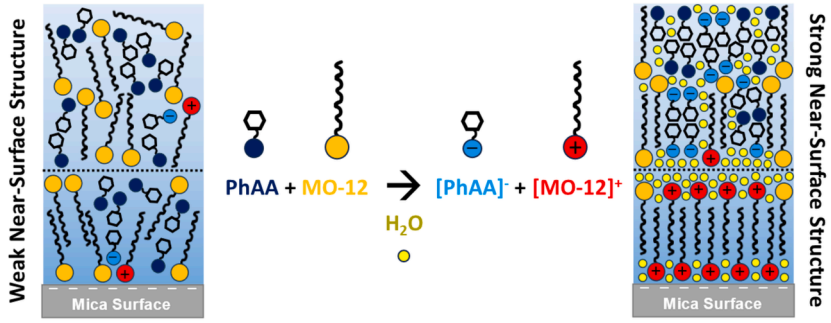

ARTICLE INFO

Keywords:
Non-ionic deep eutectic solvents
Amphiphilic
Nanostructure
Proton transfer
Lubrication
Atomic force microscopy

ABSTRACT

Hypothesis: The addition of water to a non-ionic *N*-oxide deep eutectic solvent (DES) composed of phenylacetic acid (PhAA) and *N*-dodecylmorpholine-*N*-oxide (MO-12) in a 1:1 M ratio (PhAA/MO-12) will promote interfacial nanostructure formation due to increased proton transfer and solvophobic interactions, leading to reduced friction.

Experiments: The interfacial structure and friction of PhAA/MO-12 with water content up to 41.9 wt% were investigated at mica surfaces. Atomic force microscopy (AFM) was used to measure normal force-separation profiles, lateral images, and nanoscale friction.

Findings: Conductivity increases over twentyfold with the addition of 23.6 wt% water. AFM force curves reveal that increasing water content in PhAA/MO-12 leads to a more pronounced interfacial structure with steps extending further into the bulk. High-resolution near-surface images show a well-defined sponge-like nanostructure at 23.6 wt% water, which is absent in the neat DES. The enhanced nanostructure is attributed to increased proton transfer from PhAA to MO-12 and segregation of polar and apolar domains driven by water-

Abbreviations: DESs, deep eutectic solvents; HBD, hydrogen bond donor; HBA, hydrogen bond acceptor; ChCl, choline chloride; ILs, ionic liquids; PhAA, phenylacetic acid; MO-12, *N*-dodecylmorpholine-*N*-oxide; AO-12, *N*,*N*-dimethyldodecyl-*N*-amine oxide; AFM, atomic force microscopy; A_0, free amplitude; A, set amplitude; A/A_0, amplitude setpoint ratio; 2D FFT, two-dimensional fast Fourier transform; μ, friction coefficient; [$Py_{1,4}$][TFSI], 1-butyl-1-methylpyrrolidinium bis(trifluoromethylsulfonyl)imide; [EMIm][TFSI], 1-ethyl-3-methylimidazolium bis(trifluoromethylsulfonyl)imide.

* Corresponding author at: School of Molecular Sciences, The University of Western Australia, Perth, WA 6009, Australia.
E-mail address: hua.li@uwa.edu.au (H. Li).

https://doi.org/10.1016/j.jcis.2024.12.092
Received 20 September 2024; Received in revised form 11 December 2024; Accepted 13 December 2024
Available online 16 December 2024

strengthened solvophobic interactions. Friction reduces up to 72 % for ≥7.0 wt% water compared to the neat DES, due to a more robust boundary layer facilitated by water.

1. Introduction

Ionic liquids (ILs) are pure salts that exist as liquids at or near room temperature. ILs containing alkyl chains of adequate length self-assemble into sponge-like nanostructures due to the solvophobic effect, where polar domains are formed by attractive interactions between charged moieties, and apolar domains are created by the solvophobic exclusion of alkyl chains [1]. This nanostructure enables the concurrent solubilization of both polar and non-polar substances in ILs [1]. Recent atomic force microscopy (AFM) studies on ILs [2] have shown that ILs with amphiphilic characteristics display a distinctive nanostructure in the near-surface region. In this arrangement, the top half of a near-surface aggregate moves slowly over the Stern layer. Compression of these aggregates by the AFM probe produces the characteristic steps observed in the force-separation profiles. Studies on ILs using X-ray diffraction and neutron scattering have also revealed this characteristic near-surface ordering [3,4]. The unique nanostructures and properties of ILs have enabled their widespread adoption in diverse technologies, ranging from lubricants [5], sensors [6], solar cells [7], electrolytes [8,9], and biomass processing [10,11]. However, the toxicity of many ILs and the high cost of their starting materials have prompted research into more sustainable and cost-effective alternatives [12].

Deep eutectic solvents (DESs) are composed of a hydrogen bond donor (HBD) and a hydrogen bond acceptor (HBA), mixed in a ratio that results in a melting point lower than the individual components [13]. DESs exhibit useful properties of ILs, such as tunability, while offering the advantage of being made from more cost-effective, environmentally benign, and biodegradable materials. This makes DESs attractive for various applications, including chemical syntheses [14-17], extraction [18], separation [19], gas capture [20], drug delivery [21], and nanoparticle solubilization [22].

Conventional DESs are categorized into four types based on their components [18,23-25]. Type I DESs are formed from quaternary ammonium salts (e.g., ChCl) as the HBA and metal chlorides (e.g., $FeCl_2$) as the HBD, analogous to metal halide/imidazolium ILs [26]. Type II DESs are similar, but have metal chloride hydrates as the HBD, offering lower cost and air stability which is ideal for large-scale applications. Type III DESs are composed of quaternary ammonium salts and a wider range of HBDs such as amides, carboxylic acids, and alcohols [22,27,28]. These DESs are easy to prepare, relatively stable in the presence of water, often biodegradable, and features relatively cheap starting materials. Due to these advantages, Type III DESs have attracted attention as they solvate various transition metal species [22], and their physical properties can be tuned for specific applications by choosing different HBDs. In contrast, Type IV DESs feature the same selection of HBDs but with metal chloride hydrates as the HBA, such as $ZnCl_2$ mixed with urea [29].

A new type of DES, known as Type V, was defined in 2019 based on studies of thymol-menthol mixtures [23]. Type V DESs consist exclusively of molecular substances and are formed through hydrogen bonding between a HBA and a HBD that is a hydroxyl group directly attached to an aromatic ring, such as a phenolic compound [25]. This interaction enables the design of novel non-ionic DESs with unique properties, including lower viscosities compared to ionic DESs, the absence of chloride, and measurable vapour pressures, which may be beneficial in applications requiring solvent recovery through evaporation or distillation [30,31].

Although their hydrogen bonding networks can facilitate spontaneous amphiphile self-assembly [32], conventional Type I–Type IV DESs are usually composed of short alkyl chain species, thus lack inherent amphiphilic nanostructures, which limit their wider applications. However, recent studies on DESs have shown that the use of amphiphilic components facilitates spontaneous amphiphile self-assembly, which can induce nanostructure similar to ILs [32]. This enables the creation of DESs that combine the advantageous properties of ILs with greener, more cost-effective materials. Compared to conventional Type I–Type IV DESs, Type V DESs offer greater flexibility in tuning amphiphilicity through the selection of non-ionic compounds with various alkyl chain lengths [30], and thus have great potential for a variety of applications. For instance, amphiphilic Type V DESs composed of environmentally friendly components, i.e. phenylacetic acid (PhAA) as the HBD and various *N*-oxides as the HBA [33–36], exhibit very low freezing points and polarities similar to conventional ILs [37], making them promising reaction media for chemical synthesis [38].

Water addition has been found to affect nanostructures of conventional Type I to Type IV DESs both in the bulk and at the interface. Neutron scattering and atomic force microscopy (AFM) [39,40] experiments [41] as well as molecular dynamics simulations [42–45] on Type III DESs composed of a 1:2 M ratio of ChCl and urea (reline), ChCl and ethylene glycol (ethaline), and ChCl and glycerol (glyceline) have revealed that ion arrangements are retained with up to 40 wt% water both in the bulk and at interfaces, as water molecules solvate DES components and take part in the network of hydrogen bonding. However, above 50 wt% water, these DES ions become fully solvated, resulting in a homogeneous mixture [46,47]. Adding 10 wt% water to a Type III DES with an amphiphilic HBD, ChCl:butyric acid (molar ratio 1:4), enhances the bulk nanostructure by increasing the polarity difference between charged and uncharged domains, promoting alkyl chain segregation [48]. In other Type III DESs with amphiphilic cations (ethylammonium bromide and butylammonium bromide mixed with urea), increasing the length of the cation alkyl chains results in more significant solvophobic interactions, thus more pronounced interfacial nanostructures [49].

Liquids with stronger interfacial nanostructure, especially in the Stern layer, have been found to promote lubrication [50,51], especially in the boundary regime. This makes it critical to study boundary layer lubrication of amphiphilic DESs and their water mixtures for a comprehensive understanding of their properties and potential applications. Previous studies have found that ChCl-based and menthol-based DESs are ideal lubricants, due to their strong surface adsorption, as well as the advantage of a lower synthesis cost compared to conventional ILs [52–54]. Surface force balance experiments have shown that ChCl-based DESs with 30 wt% water exhibit lubrication properties comparable to conventional ILs, attributed to water molecules strengthening polar domains and forming a more robust Stern layer [55]. However, the relationship between water content and lubrication is not always straightforward. For instance, a DES analogue composed of ChCl and magnesium chloride hexahydrate exhibits very low friction at water concentrations between 2 and 10 wt% but increased friction above 10 wt % [56]. This suggests the existence of an optimal water content range for achieving the desired lubrication performance in DESs.

To date, the interfacial structure and lubrication properties of promising amphiphilic Type V DESs, such as PhAA/*N*-oxides, remain unexplored in both neat and water-containing states, limiting their wider applications. Unlike conventional ionic DESs (Type I-Type IV) and ILs where charged species are inherently present, Type V DESs are unique in starting as purely molecular species. This fundamental difference suggests that their response to water addition could reveal new mechanisms for tuning interfacial properties. While water effects have been extensively studied in ionic systems [57–63], the potential for water to mediate a molecular-to-ionic transition in Type V DESs, and the subsequent impact on interfacial structure and properties, remains

unexplored.

To address the knowledge gap, this work investigates the interfacial nanostructure and lubrication properties of a 1:1 M ratio PhAA/*N*-dodecylmorpholine-*N*-oxide (MO-12) DES (PhAA/MO-12) with varying water content on mica substrates using AFM. MO-12 was chosen as the HBA for its relatively low hygroscopicity compared to similar *N*-oxides. The findings contribute to understanding nanostructure-friction relationships in amphiphilic non-ionic DESs, potentially guiding the development of economical, environmentally friendly lubricants and other similar applications involving interfacial phenomena.

2. Materials and methods

2.1. Chemicals and materials

Phenylacetic acid (PhAA) was purchased from Sigma–Aldrich and was used as received. *N*-dodecylmorpholine-*N*-oxide (MO-12) was synthesized using a previously published method [37].1-butyl-1-methylpyrrolidinium bis(trifluoromethylsulfonyl)imide ([$Py_{1,4}$][TFSI]) and 1-ethyl-3-methylimidazolium bis(trifluoromethylsulfonyl)imide ([EMIm][TFSI]) were obtained from IoLiTec Ionic Liquids Technologies GmbH. Milli-Q water was sourced from a Merck EQ 7000 ultrapure water system.

Mica surfaces (V-1 Grade, 15 mm) were purchased from SPI Supplies. Mica substrates were selected for their atomically smooth surfaces with well-defined negative surface charge density, which enables reliable force measurements and imaging of interfacial structures. While other substrates like silicon could potentially be used, the chemical stability and reproducible surface properties of mica make it particularly suitable for fundamental interfacial studies.

2.2. Sample preparation and characterisation

The PhAA/MO-12 DES samples were prepared by mixing the solid compounds at the proper molar ratio and heating the mixtures at 90 °C to obtain a homogenous liquid phase. MO-12 characterization was based on a previously published method [37]. ^{1}H NMR spectral data of the PhAA/MO-12 DES are presented in Fig. S1.

The neat PhAA/MO-12 sample contained 0.3 wt% water, as tested by Karl Fischer titration. Milli-Q water was added to PhAA/MO-12 to prepare samples with varying water content. Table 1 lists the prepared DES/water mixtures with the corresponding wt%. A PhAA/MO-12 sample with 50.1 wt% (95.6 mol%) water was attempted but did not form a homogeneous phase required for AFM measurements.

2.3. Conductivity measurements

Conductivity measurements were conducted with an Keysight E4980AL Precision LCR Meter with a 4-point probe Farnell LFA1107 Class B conductivity sensor. The cell constant (K) was empirically calibrated with two known ionic liquid standards, which were [$Py_{1,4}$][TFSI] and [EMIm][TFSI], and was found to be 2.83 cm^{-1}. All readings were taken at room temperature. The results of the DES/water samples together with two IL standards are listed in Table 1.

Table 1
Experimental and reported conductivities (σ) for the DES within prepared DES/water mixtures, [$Py_{1,4}$] [TFSI], [EMIm] [TFSI], and Milli-Q water. All conductivity measurements were taken with a cell constant of 2.83 cm^{-1} and at room temperature.

Sample	Experimental σ ($mS{\cdot}cm^{-1}$)	Reported σ ($mS{\cdot}cm^{-1}$)
Neat PhAA/MO-12	0.033	0.029 [37]
PhAA/MO-12 with 23.6 wt% H_2O	0.724	–
[$Py_{1,4}$] [TFSI]	2.126	2.12 [73]
[EMIm] [TFSI]	6.634	6.63 [74]
Milli-Q H_2O	–	0.000055 [75]

2.4. AFM experiments

AFM experimental protocols followed established methodologies validated in multiple peer-reviewed studies investigating similar systems [49,64–67]. Normal force-separation profiles and lateral force-normal force relationships were investigated using a Veeco Nanoscope IV AFM on a newly exposed mica surface at 22 °C) with the laboratory temperature continuously monitored and maintained by a central air conditioning system. Thermocouples were used to verify thermal equilibrium within the AFM enclosure throughout each experiment, ensuring that any observed changes in interfacial structure could be attributed to water content rather than thermal fluctuations. Sharp silicon AFM probes (NSC36 model from Mikromasch, spring constants of ~0.7 $N{\cdot}m^{-1}$) were subjected to a cleaning protocol involving ethanol and Milli-Q water, as well as a UV-Ozone treatment for 5 min prior to use. An AFM fluid cell (Bruker) was cleaned with ethanol and Milli-Q water, then dried with N_2 before each experiment. Normal force vs separation curves were acquired by advancing the surface towards the AFM probe while recording cantilever deflection with separation. The ramp size and rate of ramp are 50 to 100 nm and 0.2 Hz, respectively. Established methodologies were employed to transform deflection vs separation data into normal force vs separation curves. To measure lateral forces, the AFM was configured to scan perpendicular to the longitudinal axis of the AFM probe with the slow scan axis deactivated. The scan dimensions were 500 nm, with a scan rate of 6 Hz. A customized MATLAB function, accounting for the torsional spring constant and cantilever geometrical parameters, was utilized to convert the deflection signal in the lateral direction (cantilever twist) into lateral force [68].

Amplitude modulation AFM imaging of PhAA/MO-12 on a mica surface was measured by the Cypher VRS AFM (Asylum Research) at 60 °C. Imaging attempts below 60 °C were unsuccessful due to high viscosity of the liquid. The cantilever was excited acoustically using a piezoelectric actuator, oscillating at or near its resonant frequency. As the oscillating AFM probe approaches the mica surface, the free amplitude (A_0) is attenuated to the set amplitude (A), resulting in a phase lag of the cantilever oscillation relative to the input oscillation. A feedback loop maintains A at an approximately constant value, generating topographical and phase images. Images were acquired using an amplitude setpoint ratio (A/A_0) exceeding 0.6 [69]. The AFM probes used for imaging (AC40, Olympus) has a very low spring constant of 0.09 ± 0.02 $N{\cdot}m^{-1}$, suggesting that the obtained features in AFM images are more likely representative of the near-surface region rather than the Stern layer. The AFM probes were cleaned with ethanol and Milli-Q water, followed by UV-Ozone treatment for 5 min prior to use. Image acquisition commenced only after the system reached a stable equilibrium state. The entire imaging process was completed within a timeframe less than 4 h. Amplitude modulation imaging data underwent quantitative analysis to determine the repeat spacing of surface features using two-dimensional fast Fourier transform (2D FFT) integral transformation and the Fit Function tools in Gwyddion, a specialized AFM analysis software [70]. The obtained repeat spacing was applied to ascertain the dimension of image features, facilitating the determination of the near-surface nanostructure at solid–liquid interfaces.

To ensure measurement reliability and reproducibility, AFM cantilever spring constants were calibrated using thermal tuning prior to each force and imaging experiment. Both normal and lateral force measurements were performed at a minimum of three different locations on each surface to account for potential surface heterogeneity. A systematic approach was used when studying DES samples with different water content, in which measurements were conducted from lowest to highest water concentration to minimize contamination effects. Each experimental measurement was conducted a minimum of three times at

different surface locations to account for potential surface heterogeneities. Only measurements showing consistent behaviour across these repeated trials were included in the analysis. This approach ensures that observed changes in interfacial structure and friction are representative of genuine physical phenomena rather than artifacts from surface irregularities or probe contamination. The AFM data interpretation was validated through cross-correlation between force spectroscopy, lateral force measurements, and imaging. These measurements were further complemented by conductivity data to provide independent confirmation of structural changes.

3. Results and discussion

3.1. Conductivity

Table 1 shows the conductivity of the neat PhAA/MO-12 DES (0.033 mS cm^{-1}) is three orders of magnitude larger than that of Milli-Q water (0.000055 mS cm^{-1}). As PhAA is a weak acid (pKa = 4.31) [71] and MO-12 has a pKa close to 5.0 [72], proton transfer is limited from PhAA to MO-12 in the neat DES, resulting in mainly molecular components. However, the presence of $[PhAA]^-$ and $[MO\text{-}12]^+$ cannot be neglected, as the significant conductivity increase compared to Milli-Q water suggests a small but notable ionic portion [37].

The addition of water to the PhAA/MO-12 DES significantly increases its conductivity from 0.033 mS·cm^{-1} to 0.724 mS·cm^{-1} (Table 1), comparable to conventional ionic DESs and ILs [13,46,49,73,74]. The significant increase in conductivity upon water addition for the PhAA/MO-12 DES indicates that the added water molecules surround and hydrate PhAA and MO-12 molecules, enabling them to dissociate and interact more freely. Consequently, proton transfer from PhAA to MO-12 is facilitated, leading to higher concentrations of $[PhAA]^-$ and $[MO\text{-}12]^+$ ions comparable to conventional ionic DESs and ILs.

The dramatic conductivity increase observed in this study reveals a previously unreported mechanism in Type V DESs, where water mediates the transition from a predominantly molecular system to one with significant ionic character. This behaviour differs fundamentally from conventional ionic DESs and ILs, where water primarily affects the mobility and distribution of pre-existing ionic species.

3.2. Force-separation profiles

Fig. 1**a** shows characteristic normal force-separation profiles as an AFM probe approaches a mica surface submerged in neat PhAA/MO-12 and with water contents of 7.0 wt%, 11.6 wt%, 23.6 wt%, and 41.9 wt%. These force curves are vertically offset to enable clear visualization of the changes in interfacial structure, but all systems exhibit zero force at large separation distances. Single representative force curves are presented instead of averages, since the process of averaging multiple curves can potentially obscure or eliminate important features at low normal forces [76,77]. The exact distance between the AFM probe and the substrate cannot be achieved, as the compliance region at zero apparent separation corresponds to the AFM probe pushing against material that cannot be penetrated, which is not necessarily in contact with the substrate. The maximum force of each step, known as the push-through or rupture force, indicates the AFM probe disrupting the interfacial layer. The step numbers and the rupture force magnitude in force-separation curves generally increase with the interfacial structure of the liquid [49,76,78].

Fig. 1**a** shows that for neat PhAA/MO-12, no significant force is detected until a separation of 3.5 nm. From 3.5 nm to 1.5 nm, a monotonic increase in force to approximately 3 nN is observed, followed by a steeper increase to 12 nN at compliance. This lack of discrete steps indicates the absence of well-defined interfacial structures [39,47,51].

The first weak layer detected at 3.5 nm may be due to the AFM probe encountering some weak near-surface liquid nanostructures, likely aggregates of PhAA and MO-12, which are compressed first and then pushed through as the force exceeds 3 nN. The second layer starting at 1.5 nm, consistent with the MO-12 alkyl chain length (1.48 nm, Fig. 1**b**) [61,79], suggests the rupture of a MO-12 enriched layer. However, according to previous studies [80–82], there may exist another layer enriched in MO-12/$[MO\text{-}12]^+$ with alkyl chains towards the upper MO-12 layer, and polar heads strongly attaching to the negative mica surface via hydrogen bonding and electrostatic interactions, which cannot be pushed through. The schematic of this MO-12 bilayer structure is shown in Fig. 2**a**.

The absence of discrete steps in neat PhAA/MO-12 is different from conventional ionic DESs and ILs, where interfacial structure typically exists even without water addition due to their inherent ionic nature. This difference highlights the unique starting point of Type V DESs as molecular systems, enabling the observation of water-induced structural evolution from a truly non-ionic state.

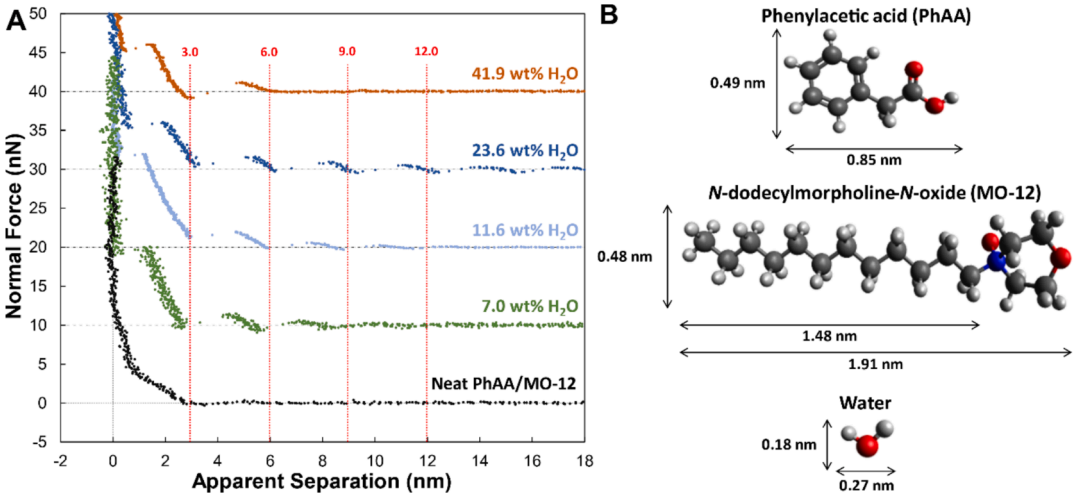

Fig. 1. (a) Typical normal force-separation profiles of a silicon AFM probe approaching a mica surface immersed in neat PhAA/MO-12 and with increasing water content at room temperature. The force curves are vertically offset for visual clarity. Key features are indicated by dotted red lines. (b) Structures and dimensions of PhAA, MO-12, and water molecules, calculated using Avogadro software [61,79]. (For interpretation of the references to colour in this figure legend, the reader is referred to the web version of this article.). (For interpretation of the references to colour in this figure legend, the reader is referred to the web version of this article.)

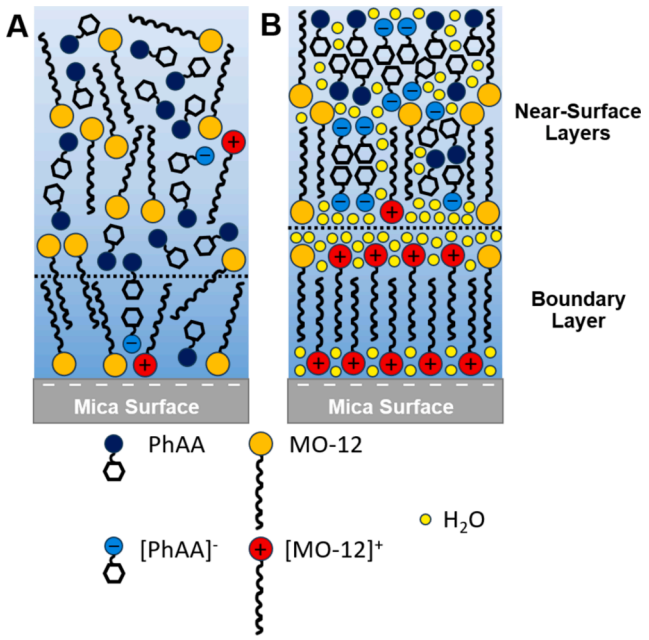

Fig. 2. Schematic illustrating the interfacial structure of (a) neat PhAA/MO-12 and (b) PhAA/MO-12 with ≥7.0 wt% water on a micra surface at the nanoscale. Note that the real structure is more intricate and constantly changing compared to that shown in the schematic.

For PhAA/MO-12 DESs with ≥7.0 wt% water, discrete steps are detected due to the AFM probe contacting structures in the near-surface region, consistent with previous studies [66,67,83–85]. As the water content increases from 7.0 wt% to 23.6 wt%, the number of steps, the separation at which forces are first detected, and the push-through forces all increase, revealing more extensive and strongly ordered interfacial nanostructures. This systematic enhancement of interfacial structure with increasing water content follows similar trends observed in conventional Type I–IV DESs, where water molecules preferentially associate with polar groups to strengthen the hydrogen bond network [39]. The addition of water also promote higher concentrations of $[PhAA]^-$ and $[MO\text{-}12]^+$ ions, as indicated by the conductivities (Section 3.1), resulting in the formation of more pronounced near-surface structures, *c.f.* Fig. 2**b**. However, as the water concentration reaches 41.9 wt%, the number of steps decreases to two, suggesting the breakdown of the nanostructures and transition toward a DES-in-water mixture where dilution weakens the cohesive interactions between DES components [46,47].

The average step width of 3.0 nm for all DES/water mixtures is larger than individual components shown in Fig. 1**b**, this instead indicates the presence of hydrated MO-12/$[MO\text{-}12]^+$ self-assembled bilayers surrounded by PhAA/$[PhAA]^-$ in the near-surface region. As mica is hydrophilic, water molecules tend to be attracted to the surface, increasing the robustness of the boundary layer and strengthening the interfacial nanostructure [41,59,86–91]. The non-vertical nature of the steps may arise from compression of the MO-12 alkyl chains by the AFM probe prior to layer rupture, or from undulations within the near-surface layers [70].

Therefore, the force-separation profiles of these DES/water mixtures can be interpreted as follows: initially, the AFM probe encounters near-surface liquid nanostructures, likely self-assembled aggregates composed of MO-12/$[MO\text{-}12]^+$ bilayers surrounded by PhAA/$[PhAA]^-$, which are compressed and then displaced when the push-through force is exceeded. Subsequently, the next detected layer is more ordered due to a higher enrichment of ions resulting in stronger electrostatic interactions, leading to a higher push-through force. This continues until the surface bound Stern layer is reached, where much stronger electrostatic interactions occur between the negatively charged mica surface and the highly ordered $[MO\text{-}12]^+$ enriched bilayers, which cannot be pushed through up to high force.

Comparable large near-surface steps resulting from solvophobic self-assembly have been observed previously for DESs and ILs [67,92,93]. AFM studies on DESs composed of ChCl and carboxylic acids on a mica surface revealed that the acid alkyl chains form a “toe-to-toe” bilayer arrangement in the near-surface structure, due to the solvophobically self-assembled apolar domains, which can be disrupted and compressed by the AFM probe [67]. Similarly, surface force balance experiments on imidazolium-based and pyrrolidinium-based ILs with C_{10} alkyl chains found the formation of bilayers at mica surfaces [94,95]. The imidazolium bilayers adopt a “toe-to-toe” arrangement, while the pyrrolidinium bilayers feature fully interdigitated alkyl chain. Additionally, the transition from monolayers to bilayers occurs at different alkyl chain lengths for the two types of ILs, with a C_6 chain length being sufficient for imidazolium cations, whereas a C_{10} chain length is needed for pyrrolidinium cations. Recent AFM studies on the mixture of one IL (1-butyl-3-methylimidazolium 1,4-bis-2-ethylhexylsulfosuccinate) with 13 vol% water shown noticeably more steps in force curves than neat the IL on both gold and steel [81], due to a transition from a curved 3D sponge-like structure to a 2D lamellar structure [70].

The observed evolution of interfacial structure with increasing water content aligns with previous studies using complementary techniques. Neutron scattering experiments by Hammond et al. [41] have shown that water molecules initially integrate into and strengthen DES hydrogen bonding networks before eventually disrupting the structure at higher concentrations. Similarly, molecular dynamics simulations by Sakpal et al. [45] demonstrate how water molecules systematically modify the spatial arrangement of DES components.

3.3. *AFM images*

AFM phase and amplitude images were taken to study the near-surface nanostructure (above the Stern layer) of PhAA/MO-12 with 23.6 wt% water at the mica surface (Fig. 3). The images were acquired at 60 °C because the high viscosity of the liquid at lower temperatures prevented the collection of high-quality AFM images. Phase images are derived from the phase lag of the cantilever response, which is related to the stiffness of the material being probed [96]. Consequently, phase images exhibit sensitivity to the liquid compliance between the AFM probe and the surface, thereby providing a more distinct visualization of near-surface structures compared to topography images. In Fig. 3**a**, the darker regions represent compliant domains that are easily compressible by the AFM probe, while the brighter areas indicate stiff, non-compliant domains. This pattern is consistent with previous observations of nanostructured ILs and DESs [67,97]. The observed features demonstrated consistent scaling and rotation in response to alterations in imaging parameters, ensuring that these features are unlikely to be artifacts of the imaging process.

Fig. 3**a** and **b** display consistent features, revealing an interconnected sponge-like nanostructure arising from the solvophobic effect. Water molecules preferentially hydrate the charge centres of the DES components, causing the expansion of polar domains [48]. The enhanced polar domains strengthen solvophobic segregation, repelling MO-12 alkyl chains into apolar domains, enabling the formation of the pronounced sponge-like nanostructure [48]. Promoted proton transfer from PhAA to MO-12 further enhances the solvophobic effect.

The bright, non-compliant areas in Fig. 3**a** correspond to polar domains enriched in water, $[PhAA]^-$ and $[MO\text{-}12]^+$ ions, as well as polar headgroups of PhAA and MO-12. These domains exhibit relatively rigid local structure due to electrostatic, solvophobic, and hydrogen bonding interactions. In contrast, the dark, compliant areas represent apolar domains composed of solvophobically excluded MO-12 alkyl chains, likely arranged in bilayer-like aggregates. The dimensions of both bright and dark domains are 3-4 nm, *c.f.* Fig. 3, which are consistent with the

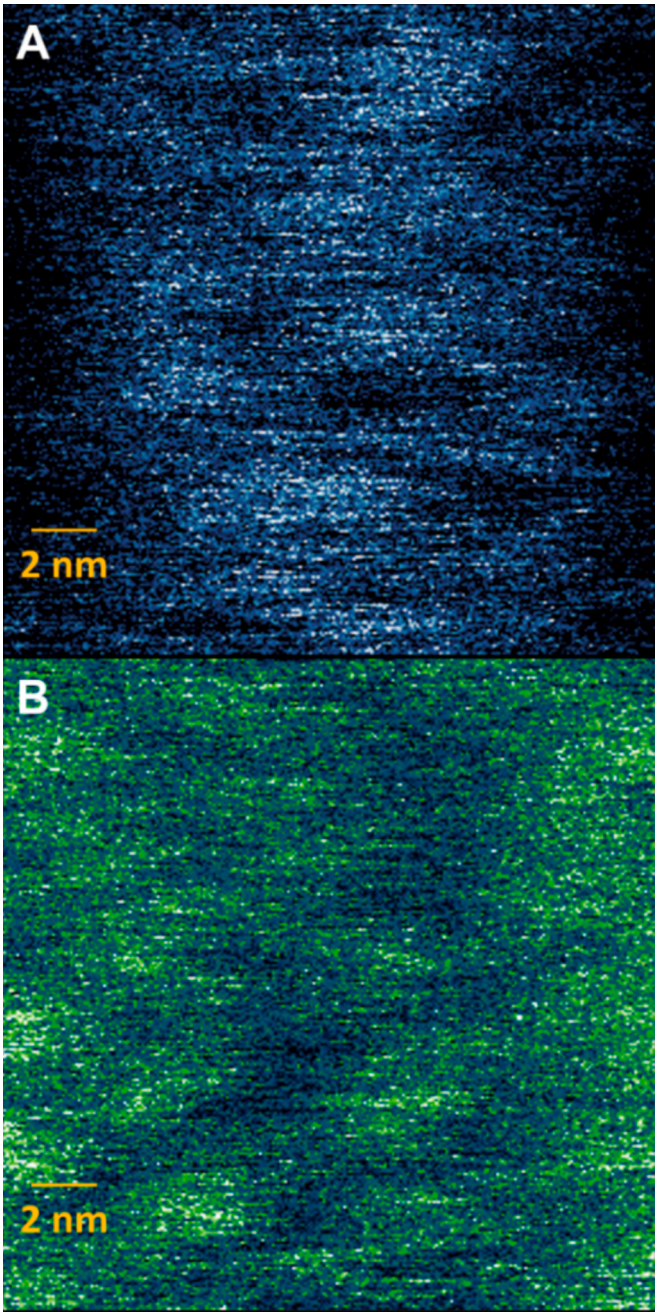

Fig. 3. 20 nm by 20 nm AM–AFM (a) phase and (b) amplitude images of PhAA/MO-12 with 23.6 wt% water on a mica surface at 60 °C.

repeat spacing of 3.3 nm extracted from both 2D FFTs (**Fig. S2**) as well as the step widths observed in the force curves (Fig. 1**a**). These structures are too large to be attributed to individual molecules or ions adsorbed in the Stern layer adsorbed to the mica surface [98], confirming the image depicts near-surface nanostructures. These findings align with previous AFM near-surface imaging studies of amphiphilically nanostructured DESs and ILs as well as their mixtures with water near a variety of surfaces [67,70,99,100].

In contrast, near-surface AFM image of neat PhAA/MO-12 (**Fig. S3**) reveal no discernible features, indicating structural homogeneity in the near-surface region, consistent with the absence of steps in the force curves (Fig. 1**a**). The lack of charged groups, such as $[PhAA]^-$ and $[MO\text{-}12]^+$ ions, in the neat DES likely weakens the solvophobic effect that drives the formation of nanostructures.

The high-resolution imaging data corelates well with force-separation profiles and conductivity measurements, strongly supporting the proposed structural evolution. This multi-technique validation approach extends established protocols for studying conventional DESs to probe the unique behaviour of Type V DES systems as well as maintaining methodological precision.

3.4. Nanoscale friction

Nanoscale friction was examined instead of macroscale friction due to its reduced susceptibility to surface asperities and roughness compared to macroscale measurements. This approach also enables the detection of molecular scale lubrication effects, which are crucial for elucidating the underlying lubrication mechanisms. AFM measured nanoscale friction mainly in the boundary lubrication regime due to the high contact pressure between the AFM probe and surface, leading to rapid removal of the bulk liquid. Consequently, the frictional response in these studies is dominated by the adsorbed boundary (Stern) layers.

Fig. 4 presents lateral (frictional) force as a function of normal force for neat PhAA/MO-12 DES and its mixtures with water content at 7.0 wt %, 11.6 wt%, 23.6 wt%, and 41.9 wt% on mica surfaces. Neat PhAA/MO-12 exhibits higher lateral forces than the DES/water mixtures across the entire normal force range investigated. A jump in lateral force is observed for neat PhAA/MO-12 at a normal force of ~10 nN, in line with the final rupture forces in the force curves (Fig. 1**a**). This sudden jump corresponds to high energy dissipation as the AFM probe breaks the boundary bilayer structure, brushing aside the top half of the MO-12 enriched layer and contacting the bottom half MO-12/$[MO\text{-}12]^+$ boundary layer, *c.f.* Fig. 2**a**, similar to previous studies [80-82]. However, this jump is less obvious for PhAA/MO-12 with ≥7.0 wt% water, which suggests that less energy is consumed as the AFM probe brushes aside the near-surface aggregates and contacts the boundary MO-12/$[MO\text{-}12]^+$ enriched bilayers, *c.f.* Fig. 2**b**, consistent with other DES/water mixtures [55].

The friction coefficient in the boundary layer regime, which is the proportionality between the lateral force and the normal force, is extracted from the gradient of the curves in Fig. 4 at normal forces >10 nN, as listed in Table 2. Neat PhAA/MO-12 exhibits the highest friction coefficient, whereas all DES/water mixtures demonstrate significantly lower values, up to a 72 % reduction, which are comparable to Type III ionic DESs (0.12–0.20) and ILs (0.14) at mica interfaces under boundary lubrication [55,67,101]. This enhanced lubrication can be attributed to a more ordered boundary layer enriched in $[MO\text{-}12]^+$ ions due to increased proton transfer leading to more pronounced solvophobic and electrostatic interactions [41,59,86,87]. Water also likely increases molecular fluidity within PhAA/MO-12 [102], allowing displaced molecules/ions to be quickly replenished and maintaining boundary layer robustness. In contrast, the absence of a well-defined interfacial

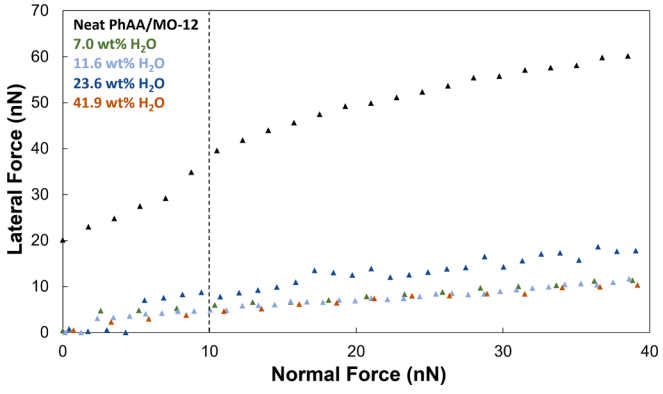

Fig. 4. Lateral force as a function of normal force for the AFM probe on mica immersed in neat PhAA/MO-12 and its mixtures with water. All measurements were taken at room temperature.

Table 2
Friction coefficients (μ) at normal force >10 nN for neat PhAA/MO-12 and its mixtures with water.

Sample	μ >10 nN
Neat PhAA/MO-12	0.69
7.0 wt% H_2O	0.20
11.6 wt% H_2O	0.21
23.6 wt% H_2O	0.32
41.9 wt% H_2O	0.19

nanostructure, especially the boundary layer, for neat PhAA/MO-12, as evidenced by the force curves and near-surface imaging, increases friction. The lack of water also hinders rapid replacement of displaced molecules, further contributing to higher friction.

This dramatic improvement in lubricity demonstrates how water can transform Type V DESs from molecular lubricants into ionic boundary lubricants with performance comparable to conventional ILs. The mechanism – whereby water promotes both proton transfer and solvophobic segregation – represents a new approach to developing sustainable lubricants that can be tuned through simple water addition.

4. Conclusion

Type V DESs have excellent properties and potential applications in extraction, drug delivery, gas capture [23,30,37]. However, to date, the interfacial structure of Type V DESs are unexplored in both neat and water-containing states, limiting their wider applications especially involving interfacial phenomena [23,30,37]. This study reveals fundamentally new insights into Type V DESs, demonstrating for the first time how water can transform their chemical nature from molecular to ionic while simultaneously promoting interfacial nanostructure formation. The conductivity has been found to increase over twentyfold from 0.033 $mS{\cdot}cm^{-1}$ to 0.724 $mS{\cdot}cm^{-1}$ with 23.6 wt% water addition, which provides direct experimental evidence for enhanced ion mobility and concentration and suggests increased proton transfer from PhAA to MO-12 in the presence of water [37]. This increase in ion concentration enhances electrostatic interactions and thus interfacial nanostructure, as demonstrated by the systematic evolution from unstructured neat DES to well-defined sponge-like morphology at 23.6 wt% water, evidenced consistently across force curves, AFM imaging, and 2D FFT analysis. The increased lubricity with water content compared to the neat DES, as detailed in the nanoscale friction tests, suggests the formation of a more robust boundary layer, likely because water molecules facilitate the enrichment and replenishment of $[MO\text{-}12]^+$ ions at the interface.

These findings provide insight into the relationship between the composition, nanostructure, and tribological performance in amphiphilic DES systems, creating a new pathway for the development of Type V DESs in various applications, particularly as economical, environmentally friendly lubricants. Future molecular dynamics simulations will aid understanding of precise spatial distribution and dynamics of PhAA, MO-12 and water molecules in both bulk and at the interface, as well as the impact of water content on proton transfer between PhAA and MO-12, and interfacial nanostructure.

Declaration of Generative AI and AI-assisted technologies in the writing process

During the preparation of this work, the authors used Claude in order to improve language. After using this service, the authors reviewed and edited the content as needed and take full responsibility for the content of the publication.

CRediT authorship contribution statement

Joshua J. Buzolic: Writing – review & editing, Writing – original draft, Methodology, Investigation, Formal analysis, Data curation, Conceptualization. **Matteo Tiecco:** Writing – review & editing, Resources, Methodology. **Rob Atkin:** Writing – review & editing, Supervision, Resources, Project administration, Funding acquisition, Conceptualization. **Hua Li:** Writing – review & editing, Writing – original draft, Supervision, Resources, Methodology, Conceptualization.

Declaration of competing interest

The authors declare that they have no known competing financial interests or personal relationships that could have appeared to influence the work reported in this paper.

Acknowledgements

JJB thanks the support from an Australian Government Research Training Program Scholarship at The University of Western Australia. The authors acknowledge the facilities and the scientific and technical assistance of the Australian Microscopy & Microanalysis Research Facility at the Centre for Microscopy, Characterisation & Analysis, The University of Western Australia; a facility funded by the University, and the State and Commonwealth Governments. This work was supported by an Australian Research Council Discovery Project (DP200102248). JJB thanks Simone Ciampi for access to the LCR Meter for conductivity measurements, and Lucas Wong, Zahra M. Tahroudi, Zahra Nazar, Shaik S. Hossain, and Ho Hong Chau for helpful comments.

Appendix A. Supplementary data

Supplementary data to this article can be found online at https://doi.org/10.1016/j.jcis.2024.12.092.

Data availability

Data will be made available on request.

References

[1] S. McDonald, T. Murphy, S. Imberti, G.G. Warr, R. Atkin, Amphiphilically nanostructured deep eutectic solvents, J. Phys. Chem. Lett 9 (2018) 3922–3927, https://doi.org/10.1021/acs.jpclett.8b01720.
[2] H. Li, J. Wang, G.G. Warr, R. Atkin, Extremely slow dynamics of ionic liquid self-assembled nanostructures near a solid surface, J. Colloid Interface Sci. 630 (2023) 658–665, https://doi.org/10.1016/j.jcis.2022.10.123.
[3] D. Noferini, O. Holderer, H. Frielinghaus, Effect of mild nanoscopic confinement on the dynamics of ionic liquids, Phys. Chem. Chem. Phys. 22 (2020) 9046–9052, https://doi.org/10.1039/C9CP05200C.
[4] H. Frielinghaus, M. Fomina, D. Hayward, P.S. Dubey, S. Jaksch, P. Falus, P. Fouquet, L. Fruhner, O. Holderer, Ionic Liquid (EmimAc)-water mixture confined in nanoporous glass matrices studied with high-resolution neutron spectroscopy, Front. Phys. 10 (2022), https://doi.org/10.3389/fphy.2022.872616.
[5] R. Lhermerout, C. Diederichs, S. Perkin, Are ionic liquids good boundary lubricants? A molecular perspective, Lubricants 6 (2018) 9, https://doi.org/10.3390/lubricants6010009.
[6] D.S. Silvester, New innovations in ionic liquid–based miniaturised amperometric gas sensors, Curr. Opin. Electrochem. 15 (2019) 7–17, https://doi.org/10.1016/j.coelec.2019.03.001.
[7] D.R. Macfarlane, N. Tachikawa, M. Forsyth, J.M. Pringle, P.C. Howlett, G. D. Elliott, J.H. Davis, M. Watanabe, P. Simon, C.A. Angell, Energy applications of ionic liquids, Energy Environ. Sci. 7 (2014) 232–250, https://doi.org/10.1039/c3ee42099j.
[8] D.S. Silvester, R. Jamil, S. Doblinger, Y. Zhang, R. Atkin, H. Li, Electrical double layer structure in ionic liquids and its importance for supercapacitor, battery, sensing, and lubrication applications, J. Phys. Chem. C 125 (2021) 13707–13720, https://doi.org/10.1021/acs.jpcc.1c03253.
[9] J. Wang, J.J. Buzolic, J.W. Mullen, P.A. Fitzgerald, Z.M. Aman, M. Forsyth, H. Li, D.S. Silvester, G.G. Warr, R. Atkin, Nanostructure of locally concentrated ionic liquids in the bulk and at graphite and gold electrodes, ACS Nano 17 (2023) 21567–21584, https://doi.org/10.1021/acsnano.3c06609.
[10] S.S.Y. Tan, D.R. MacFarlane, Ionic liquids in biomass processing, Top Curr. Chem. 290 (2009) 311–339, https://doi.org/10.1007/128_2008_35.

[11] L.N. Wong, M. Brunner, S. Imberti, G.G. Warr, R. Atkin, Bulk nanostructure of mixtures of choline arginate, choline lysinate, and water, J. Phys. Chem. B 128 (2024) 4853–4863, https://doi.org/10.1021/acs.jpcb.4c01482.
[12] R. Hayes, G.G. Warr, R. Atkin, Structure and nanostructure in ionic liquids, Chem. Rev. 115 (2015) 6357–6426, https://doi.org/10.1021/cr500411q.
[13] A.P. Abbott, D. Boothby, G. Capper, D.L. Davies, R.K. Rasheed, Deep Eutectic Solvents formed between choline chloride and carboxylic acids: Versatile alternatives to ionic liquids, J. Am. Chem. Soc. 126 (2004) 9142–9147, https://doi.org/10.1021/ja048266j.
[14] Y. Dai, J. van Spronsen, G.J. Witkamp, R. Verpoorte, Y.H. Choi, Natural deep eutectic solvents as new potential media for green technology, Anal. Chim. Acta 766 (2013) 61–68, https://doi.org/10.1016/j.aca.2012.12.019.
[15] P. Liu, J.W. Hao, L.P. Mo, Z.H. Zhang, Recent advances in the application of deep eutectic solvents as sustainable media as well as catalysts in organic reactions, RSC Adv. 5 (2015) 48675–48704, https://doi.org/10.1039/c5ra05746a.
[16] M. Tiecco, R. Germani, F. Cardellini, Carbon-carbon bond formation in acid deep eutectic solvent: Chalcones synthesis: Via Claisen-Schmidt reaction, RSC Adv. 6 (2016) 43740–43747, https://doi.org/10.1039/c6ra04721a.
[17] D.A. Alonso, A. Baeza, R. Chinchilla, G. Guillena, I.M. Pastor, D.J. Ramón, Deep eutectic solvents: the organic reaction medium of the century, Eur. J. Org. Chem. 2016 (2016) 612–632, https://doi.org/10.1002/ejoc.201501197.
[18] E.L. Smith, A.P. Abbott, K.S. Ryder, Deep Eutectic Solvents (DESs) and their applications, Chem. Rev. 114 (2014) 11060–11082, https://doi.org/10.1021/cr300162p.
[19] A. Paiva, R. Craveiro, I. Aroso, M. Martins, R.L. Reis, A.R.C. Duarte, Natural deep eutectic solvents - solvents for the 21st century, ACS Sustain. Chem. Eng. 2 (2014) 1063–1071, https://doi.org/10.1021/sc500096j.
[20] T. Homan, K. Shahbaz, M.M. Farid, Improving the production of propyl and butyl ester-based biodiesel by purification using deep eutectic solvents, Sep. Purif. Technol. 174 (2017) 570–576, https://doi.org/10.1016/j.seppur.2016.10.036.
[21] H. Zhang, X. Qiao, T. Cai, J. Chen, Z. Li, H. Qiu, Preparation and characterization of carbon dot-decorated silica stationary phase in deep eutectic solvents for hydrophilic interaction chromatography, Anal. Bioanal. Chem. 409 (2017) 2401–2410, https://doi.org/10.1007/s00216-017-0187-z.
[22] A.P. Abbott, G. Capper, D.L. Davies, K.J. McKenzie, S.U. Obi, Solubility of metal oxides in deep eutectic solvents based on choline chloride, J. Chem. Eng. Data 51 (2006) 1280–1282, https://doi.org/10.1021/je060038c.
[23] D.O. Abranches, M.A.R. Martins, L.P. Silva, N. Schaeffer, S.P. Pinho, J.A. P. Coutinho, Phenolic hydrogen bond donors in the formation of non-ionic deep eutectic solvents: the quest for type V DES, Chem. Commun. 55 (2019) 10253–10256, https://doi.org/10.1039/C9CC04846D.
[24] D.O. Abranches, J.A.P. Coutinho, Everything you wanted to know about deep eutectic solvents but were afraid to be told, Annu. Rev. Chem. Biomol. Eng. 14 (2023) 141–163, https://doi.org/10.1146/annurev-chembioeng-101121-085323.
[25] D.J.G.P. van Osch, C.H.J.T. Dietz, S.E.E. Warrag, M.C. Kroon, The curious case of hydrophobic deep eutectic solvents: a story on the discovery, design, and applications, ACS Sustain. Chem. Eng. 8 (2020), https://doi.org/10.1021/acssuschemeng.0c00559.
[26] M.S. Sitze, E.R. Schreiter, E.V. Patterson, R.G. Freeman, Ionic liquids based on FeCl3 and FeCl2. Raman scattering and ab initio calculations, Inorg. Chem. 40 (2001) 2298–2304, https://doi.org/10.1021/ic001042r.
[27] A.P. Abbott, T.J. Bell, S. Handa, B. Stoddart, Cationic functionalisation of cellulose using a choline based ionic liquid analogue, Green Chem. 8 (2006) 784–786, https://doi.org/10.1039/b605258d.
[28] A.P. Abbott, P.M. Cullis, M.J. Gibson, R.C. Harris, E. Raven, Extraction of glycerol from biodiesel into a eutectic based ionic liquid, Green Chem. 9 (2007) 868–887, https://doi.org/10.1039/b702833d.
[29] A.P. Abbott, J.C. Barron, K.S. Ryder, D. Wilson, Eutectic-based ionic liquids with metal-containing anions and cations, Chem. Eur. J. 13 (2007) 6495–6501, https://doi.org/10.1002/chem.200601738.
[30] D.O. Abranches, J.A.P. Coutinho, Type V deep eutectic solvents: design and applications, Curr. Opin. Green Sustain. Chem. 35 (2022) 100612, https://doi.org/10.1016/j.cogsc.2022.100612.
[31] J. Potticary, C. Hall, V. Hamilton, J.F. McCabe, S.R. Hall, Crystallization from volatile deep eutectic solvents, Cryst. Growth Des. 20 (2020) 2877–2884, https://doi.org/10.1021/acs.cgd.0c00399.
[32] S.J. Bryant, R. Atkin, G.G. Warr, Spontaneous vesicle formation in a deep eutectic solvent, Soft Matter 12 (2016) 1645–1648, https://doi.org/10.1039/c5sm02660a.
[33] F. Wightman, D.L. Lighty, Identification of phenylacetic acid as a natural auxin in the shoots of higher plants, Physiol. Plant. 55 (1982) 17–24, https://doi.org/10.1111/j.1399-3054.1982.tb00278.x.
[34] E. Anklam, A review of the analytical methods to determine the geographical and botanical origin of honey, Food Chem. 63 (1998) 549–562, https://doi.org/10.1016/S0308-8146(98)00057-0.
[35] K. Pyrzynska, M. Biesaga, Analysis of phenolic acids and flavonoids in honey, Trends Anal. Chem. 28 (2009) 893–902, https://doi.org/10.1016/j.trac.2009.03.015.
[36] M.T. García, E. Campos, I. Ribosa, Biodegradability and ecotoxicity of amine oxide based surfactants, Chemosphere 69 (2007) 1574–1578, https://doi.org/10.1016/j.chemosphere.2007.05.089.
[37] R. Germani, M. Orlandini, M. Tiecco, T. Del Giacco, Novel low viscous, green and amphiphilic N-oxides/phenylacetic acid based Deep Eutectic Solvents, J. Mol. Liq. 240 (2017) 233–239, https://doi.org/10.1016/j.molliq.2017.05.084.
[38] E. Brambilla, A. Bortolla, V. Pirovano, A. Caselli, M. Tiecco, G. Abbiati, Silver-catalysed A3-coupling reactions in phenylacetic acid/alkylamine N-oxide eutectic mixture under dielectric heating: an alternative approach to propargylamines, Appl. Organomet. Chem. 36 (2022), https://doi.org/10.1002/aoc.6669.
[39] O.S. Hammond, H. Li, C. Westermann, A.Y.M. Al-Murshedi, F. Endres, A. P. Abbott, G.G. Warr, K.J. Edler, R. Atkin, Nanostructure of the deep eutectic solvent/platinum electrode interface as a function of potential and water content, Nanoscale Horiz. 4 (2019) 158–168, https://doi.org/10.1039/c8nh00272j.
[40] J.S. Freeman, M.H. Mamme, J. Ustarroz, G.G. Warr, H. Li, R. Atkin, Molecular resolution nanostructure and dynamics of the deep eutectic solvent—graphite interface as a function of potential, Small (2023) 2204993, https://doi.org/10.1002/smll.202204993.
[41] O.S. Hammond, D.T. Bowron, K.J. Edler, The effect of water upon deep eutectic solvent nanostructure: an unusual transition from ionic mixture to aqueous solution, Angew. Chem., Int. Ed. 56 (2017) 9782–9785, https://doi.org/10.1002/anie.201702486.
[42] S. Sarkar, A. Maity, R. Chakrabarti, Microscopic structural features of water in aqueous-reline mixtures of varying compositions, Phys. Chem. Chem. Phys. 23 (2021) 3779–3793, https://doi.org/10.1039/d0cp05341d.
[43] A.T. Celebi, T.J.H. Vlugt, O.A. Moultos, Structural, thermodynamic, and transport properties of aqueous reline and ethaline solutions from molecular dynamics simulations, J. Phys. Chem. B 123 (2019) 11014–11025, https://doi.org/10.1021/acs.jpcb.9b09729.
[44] A. Elbourne, Q.A. Besford, N. Meftahi, R.J. Crawford, T. Daeneke, T.L. Greaves, C. F. McConville, G. Bryant, S.J. Bryant, A.J. Christofferson, The impact of water on the lateral nanostructure of a deep eutectic solvent–solid interface, Aust. J. Chem. 75 (2021) 111–125, https://doi.org/10.1071/CH21078.
[45] S.S. Sakpal, S.H. Deshmukh, S. Chatterjee, D. Ghosh, S. Bagchi, Transition of a deep eutectic solution to aqueous solution: a dynamical perspective of the dissolved solute, J. Phys. Chem. Lett. 12 (2021) 8784–8789, https://doi.org/10.1021/acs.jpclett.1c02118.
[46] Y. Dai, G.J. Witkamp, R. Verpoorte, Y.H. Choi, Tailoring properties of natural deep eutectic solvents with water to facilitate their applications, Food Chem. 187 (2015) 14–19, https://doi.org/10.1016/j.foodchem.2015.03.123.
[47] O.S. Hammond, D.T. Bowron, A.J. Jackson, T. Arnold, A. Sanchez-Fernandez, N. Tsapatsaris, V. Garcia Sakai, K.J. Edler, Resilience of malic acid natural deep eutectic solvent nanostructure to solidification and hydration, J. Phys. Chem. B 121 (2017) 7473–7483, https://doi.org/10.1021/acs.jpcb.7b05454.
[48] L.N. Wong, Silvia. Imberti, G.G. Warr, Rob. Atkin, Bulk nanostructure of a deep eutectic solvent with an amphiphilic hydrogen bond donor, Phys. Chem. Chem. Phys. 25 (2023) 31068–31076, https://doi.org/10.1039/D3CP03587E.
[49] Z. Chen, M. Ludwig, G.G. Warr, R. Atkin, Effect of cation alkyl chain length on surface forces and physical properties in deep eutectic solvents, J. Colloid Interface Sci. 494 (2017) 373–379, https://doi.org/10.1016/j.jcis.2017.01.109.
[50] P.K. Cooper, H. Li, M.W. Rutland, G.B. Webber, R. Atkin, Tribotronic control of friction in oil-based lubricants with ionic liquid additives, Phys. Chem. Chem. Phys. 18 (2016) 23657–23662, https://doi.org/10.1039/c6cp04405k.
[51] P.K. Cooper, C.J. Wear, H. Li, R. Atkin, Ionic liquid lubrication of stainless steel: friction is inversely correlated with interfacial liquid nanostructure, ACS Sustain. Chem. Eng. 5 (2017) 11737–11743, https://doi.org/10.1021/acssuschemeng.7b03262.
[52] M.T. Donato, R. Colaço, L.C. Branco, B. Saramago, A review on alternative lubricants: ionic liquids as additives and deep eutectic solvents, J. Mol. Liq. 333 (2021) 116004, https://doi.org/10.1016/j.molliq.2021.116004.
[53] A.P. Abbott, E.I. Ahmed, R.C. Harris, K.S. Ryder, Evaluating water miscible deep eutectic solvents (DESs) and ionic liquids as potential lubricants, Green Chem. 16 (2014) 4156–4161, https://doi.org/10.1039/c4gc00952e.
[54] Y. Li, C. Cao, M. Cai, H. Li, X. Fan, Y. Gao, Z. Lu, M. Zhu, Green hydrophobic deep eutectic solvents as low-viscosity and efficient lubricants, Tribol. Int. 185 (2023) 108531, https://doi.org/10.1016/j.triboint.2023.108531.
[55] J.E. Hallett, H.J. Hayler, S. Perkin, Nanolubrication in deep eutectic solvents, Phys. Chem. Chem. Phys. 22 (2020) 20253–20264, https://doi.org/10.1039/d0cp03787g.
[56] H. Liang, T. Yin, M. Liu, C. Fu, X. Xia, S. Zou, X. Hua, Y. Fu, Y. Bu, Unravelling high-load superlubricity of ionic liquid analogues by in situ Raman: incomplete hydration induced by competitive exchange of external water with crystalline water, J. Phys. Chem. Lett. 14 (2023) 453–459, https://doi.org/10.1021/acs.jpclett.2c03667.
[57] R. Hayes, S. Imberti, G.G. Warr, R. Atkin, How water dissolves in protic ionic liquids, Angew. Chem., Int. Ed. 51 (2012) 7468–7471, https://doi.org/10.1002/anie.201201973.
[58] S. Kawada, E. Kodama, K. Sato, S. Ogawa, M. Watanabe, H. Okubo, S. Sasaki, Effect of water on the interfacial structures of room-temperature ionic liquids, Surf. Interface Anal. 51 (2019) 17–20, https://doi.org/10.1002/sia.6536.
[59] C. Ma, A. Laaksonen, C. Liu, X. Lu, X. Ji, The peculiar effect of water on ionic liquids and deep eutectic solvents, Chem. Soc. Rev. 47 (2018) 8685–8720, https://doi.org/10.1039/c8cs00325d.
[60] D. Wakeham, G.G. Warr, R. Atkin, Surfactant adsorption at the surface of mixed ionic liquids and ionic liquid water mixtures, Langmuir 28 (2012) 13224–13231, https://doi.org/10.1021/la302184h.
[61] R.M. Espinosa-Marzal, A. Arcifa, A. Rossi, N.D. Spencer, Ionic liquids confined in hydrophilic nanocontacts: structure and lubricity in the presence of water, J. Phys. Chem. C 118 (2014) 6491–6503, https://doi.org/10.1021/jp5000123.
[62] H. Abe, T. Takekiyo, Y. Yoshimura, A. Shimizu, Static and dynamic properties of nano-confined water in room-temperature ionic liquids, J. Mol. Liq. 290 (2019) 111216, https://doi.org/10.1016/j.molliq.2019.111216.

[63] G. Feng, X. Jiang, R. Qiao, A.A. Kornyshev, Water in ionic liquids at electrified interfaces: the anatomy of electrosorption, ACS Nano 8 (2014) 11685–11694, https://doi.org/10.1021/nn505017c.
[64] J. Wang, X. Zhang, C. Wang, H. Li, H. Li, S. Keller, U.K. Mishra, B.D. Nener, G. Parish, R. Atkin, pH-dependent surface properties of the gallium nitride – solution interface mapped by surfactant adsorption, J. Colloid Interface Sci. 556 (2019) 680–688, https://doi.org/10.1016/j.jcis.2019.08.079.
[65] H. Li, Y. Zhang, S. Jones, R. Segalman, G.G. Warr, R. Atkin, Interfacial nanostructure and friction of a polymeric ionic liquid-ionic liquid mixture as a function of potential at Au(1 1 1) electrode interface, J. Colloid Interface Sci. 606 (2022) 1170–1178, https://doi.org/10.1016/j.jcis.2021.08.067.
[66] Y. Zhang, J.B. Marlow, W. Millar, Z.M. Aman, D.S. Silvester, G.G. Warr, R. Atkin, H. Li, Nanostructure, electrochemistry and potential-dependent lubricity of the catanionic surface-active ionic liquid [P6,6,6,14] [AOT], J. Colloid Interface Sci. 608 (2022) 2120–2130, https://doi.org/10.1016/j.jcis.2021.10.120.
[67] J.J. Buzolic, H. Li, Z. Aman, G.G. Warr, R. Atkin, Self-assembled nanostructure induced in deep eutectic solvents via an amphiphilic hydrogen bond donor, J. Colloid Interface Sci. 616 (2022) 121–128, https://doi.org/10.1016/j.jcis.2022.02.029.
[68] U.D. Schwarz, P. Köster, R. Wiesendanger, Quantitative analysis of lateral force microscopy experiments, Rev. Sci. Instrum. 67 (1996) 2560–2567, https://doi.org/10.1063/1.1147214.
[69] S. McDonald, A. Elbourne, G.G. Warr, R. Atkin, Metal ion adsorption at the ionic liquid-mica interface, Nanoscale 8 (2016) 906–914, https://doi.org/10.1039/c5nr05833c.
[70] M.J. Wydro, G.G. Warr, R. Atkin, Amplitude-modulated atomic force microscopy reveals the near surface nanostructure of surfactant sponge (L3) and lamellar (Lα) phases, Langmuir 31 (2015) 5513–5520, https://doi.org/10.1021/acs.langmuir.5b01008.
[71] W.M. Haynes, CRC Handbook of Chemistry and Physics, CRC Press, 2016 doi: 10.1201/9781315380476.
[72] G.Y. Jung, T.H. Kim, H.B. Lim, Separation of morpholine, N-methylmorpholine and N-methylmorpholine-N-oxide by indirect UV absorption capillary electrophoresis, Anal. Sci. 12 (1996) 367–370, https://doi.org/10.2116/analsci.12.367.
[73] 1-Butyl-1-methylpyrrolidinium bis(trifluoromethylsulfonyl)imide, 99.5% | IoLiTec, IoLiTec (n.d.). <https://iolitec.de/en/node/316> (Accessed July 30, 2024).
[74] 1-Ethyl-3-methylimidazolium bis(trifluoromethylsulfonyl)imide, 99.5% | IoLiTec, IoLiTec (n.d.). <https://iolitec.de/en/node/455> (Accessed July 30, 2024).
[75] Milli-Q® EQ 7000 ultrapure water system with touchscreen | ZEQ7000T0C, Merck (n.d.). <https://www.merckmillipore.com/AU/en/product/Milli-Q-EQ-7000-ultrapure-water-system-with-touchscreen,MM_NF-ZEQ7000T0C> (Accessed July 30, 2024).
[76] Z. Chen, B. McLean, M. Ludwig, R. Stefanovic, G.G. Warr, G.B. Webber, A.J. Page, R. Atkin, Nanostructure of deep eutectic solvents at graphite electrode interfaces as a function of potential, J. Phys. Chem. C 120 (2016) 2225–2233, https://doi.org/10.1021/acs.jpcc.5b10624.
[77] B. McLean, H. Li, R. Stefanovic, R.J. Wood, G.B. Webber, K. Ueno, M. Watanabe, G.G. Warr, A. Page, R. Atkin, Nanostructure of [Li(G4)] TFSI and [Li(G4)] NO3 solvate ionic liquids at HOPG and Au(111) electrode interfaces as a function of potential, Phys. Chem. Chem. Phys. 17 (2015) 325–333, https://doi.org/10.1039/c4cp04522j.
[78] R.G. Horn, D.F. Evans, B.W. Ninham, Double-layer and solvation forces measured in a molten salt and its mixtures with water, J. Phys. Chem. 92 (1988) 3531–3537, https://doi.org/10.1021/j100323a042.
[79] M.D. Hanwell, D.E. Curtis, D.C. Lonie, T. Vandermeerschd, E. Zurek, G. R. Hutchison, Avogadro: an advanced semantic chemical editor, visualization, and analysis platform, J. Cheminform. 4 (2012) 1–17, https://doi.org/10.1186/1758-2946-4-17.
[80] H. Li, T. Niemann, R. Ludwig, R. Atkin, Effect of hydrogen bonding between ions of like charge on the boundary layer friction of hydroxy-functionalized ionic liquids, J. Phys. Chem. Lett. 11 (2020) 3905–3910, https://doi.org/10.1021/acs.jpclett.0c00689.
[81] Y. Zhang, J.B. Marlow, K. Wood, J. Wang, G.G. Warr, H. Li, R. Atkin, Phase behaviour and aggregate structures of the surface-active ionic liquid [BMIm][AOT] in water, J. Colloid Interface Sci. 652 (2023) 749–757, https://doi.org/10.1016/j.jcis.2023.08.049.
[82] Y. Zhang, J.B. Marlow, W. Millar, D.S. Silvester, G.G. Warr, H. Li, R. Atkin, Effect of ion structure on the nanostructure and electrochemistry of surface active ionic liquids, J. Colloid Interface Sci. 630 (2023) 931–939, https://doi.org/10.1016/j.jcis.2022.10.074.
[83] H. Li, F. Endres, R. Atkin, Effect of alkyl chain length and anion species on the interfacial nanostructure of ionic liquids at the Au(111)-ionic liquid interface as a function of potential, Phys. Chem. Chem. Phys. 15 (2013) 14624–14633, https://doi.org/10.1039/c3cp52421c.
[84] T. Niemann, H. Li, G.G. Warr, R. Ludwig, R. Atkin, Influence of hydrogen bonding between ions of like charge on the ionic liquid interfacial structure at a mica surface, J. Phys. Chem. Lett. 10 (2019) 7368–7373, https://doi.org/10.1021/acs.jpclett.9b03007.
[85] R. Hayes, G.G. Warr, R. Atkin, At the interface: solvation and designing ionic liquids, Phys. Chem. Chem. Phys. 12 (2010) 1709, https://doi.org/10.1039/b920393a.
[86] N.F.A. Van Der Vegt, K. Haldrup, S. Roke, J. Zheng, M. Lund, H.J. Bakker, Water-mediated ion pairing: occurrence and relevance, Chem. Rev. 116 (2016) 7626–7641, https://doi.org/10.1021/acs.chemrev.5b00742.
[87] H. Kivelä, M. Salomäki, P. Vainikka, E. Mäkilä, F. Poletti, S. Ruggeri, F. Terzi, J. Lukkari, Effect of water on a hydrophobic deep eutectic solvent, J. Phys. Chem. B 126 (2022) 513–527, https://doi.org/10.1021/acs.jpcb.1c08170.
[88] M. Han, R.M. Espinosa-Marzal, Influence of water on structure, dynamics, and electrostatics of hydrophilic and hydrophobic ionic liquids in charged and hydrophilic confinement between mica surfaces, ACS Appl. Mater. Interfaces 11 (2019) 33465–33477, https://doi.org/10.1021/acsami.9b10923.
[89] A. Faghihnejad, H. Zeng, Interaction mechanism between hydrophobic and hydrophilic surfaces: using polystyrene and mica as a model system, Langmuir 29 (2013) 12443–12451, https://doi.org/10.1021/la402244h.
[90] J.J. Buzolic, H. Li, Z.M. Aman, D.S. Silvester, R. Atkin, Surface-active ionic liquids as lubricant additives to hexadecane and diethyl succinate, Colloids Surf. A: Physicochem. Eng. Asp. 699 (2024) 134669, https://doi.org/10.1016/j.colsurfa.2024.134669.
[91] F. Gabriele, M. Chiarini, R. Germani, M. Tiecco, N. Spreti, Effect of water addition on choline chloride/glycol deep eutectic solvents: Characterization of their structural and physicochemical properties, J. Mol. Liq. 291 (2019) 111301, https://doi.org/10.1016/j.molliq.2019.111301.
[92] R. Atkin, L.M. De Fina, U. Kiederling, G.G. Warr, Structure and self assembly of pluronic amphiphiles in ethylammonium nitrate and at the silica surface, J. Phys. Chem. B 113 (2009) 12201–12213, https://doi.org/10.1021/jp9063627.
[93] K. Umeda, K. Kobayashi, H. Yamada, Nanomechanics of self-assembled surfactants revealed by frequency-modulation atomic force microscopy, Nanoscale 14 (2022) 4626–4634, https://doi.org/10.1039/d2nr00369d.
[94] A.M. Smith, K.R.J. Lovelock, N.N. Gosvami, P. Licence, A. Dolan, T. Welton, S. Perkin, Monolayer to bilayer structural transition in confined pyrrolidinium-based ionic liquids, J. Phys. Chem. Lett. 4 (2013) 378–382, https://doi.org/10.1021/jz301965d.
[95] A.M. Smith, K.R.J. Lovelock, S. Perkin, Monolayer and bilayer structures in ionic liquids and their mixtures confined to nano-films, Faraday Discuss. 167 (2013) 279–292, https://doi.org/10.1039/c3fd00075c.
[96] K. Voïtchovsky, J.J. Kuna, S.A. Contera, E. Tosatti, F. Stellacci, Direct mapping of the solid-liquid adhesion energy with subnanometre resolution, Nat. Nanotechnol. 5 (2010) 401–405, https://doi.org/10.1038/nnano.2010.67.
[97] A. Elbourne, S. Cronshaw, K. Voïtchovsky, G.G. Warr, R. Atkin, Near surface properties of mixtures of propylammonium nitrate with n-alkanols 1. Nanostructure, Phys. Chem. Chem. Phys. 17 (2015) 26621–26628, https://doi.org/10.1039/c5cp04786b.
[98] A. Elbourne, S. McDonald, K. Voïchovsky, F. Endres, G.G. Warr, R. Atkin, Nanostructure of the ionic liquid-graphite stern layer, ACS Nano 9 (2015) 7608–7620, https://doi.org/10.1021/acsnano.5b02921.
[99] Z. Wang, H. Li, R. Atkin, C. Priest, Influence of water on the interfacial nanostructure and wetting of [Rmim][NTf2] ionic liquids at mica surfaces, Langmuir 32 (2016) 8818–8825, https://doi.org/10.1021/acs.langmuir.6b01790.
[100] A.J. Page, A. Elbourne, R. Stefanovic, M.A. Addicoat, G.G. Warr, K. Voïtchovsky, R. Atkin, 3-Dimensional atomic scale structure of the ionic liquid-graphite interface elucidated by AM-AFM and quantum chemical simulations, Nanoscale 6 (2014) 8100–8106, https://doi.org/10.1039/c4nr01219d.
[101] O. Werzer, E.D. Cranston, G.G. Warr, R. Atkin, M.W. Rutland, Ionic liquid nanotribology: mica-silica interactions in ethylammonium nitrate, Phys. Chem. Chem. Phys. 14 (2012) 5147–5152, https://doi.org/10.1039/c1cp23134k.
[102] E. Picciolini, G. Pastore, T. Del Giacco, G. Ciancaleoni, M. Tiecco, R. Germani, aquo-DESs: water-based binary natural deep eutectic solvents, J. Mol. Liq. 383 (2023), https://doi.org/10.1016/j.molliq.2023.122057.